Chemical stability of caesium iodide deposits in air/steam atmosphere

Dorel Obada, Houssam Hijazi, Jean-François Paul, Laurent Gasnot, Anne Cecile Gregoire, Anne Sophie Mamede, Laurent Cantrel

Chemical stability of caesium iodide deposits in air/steam atmosphere

D. Obada[a,b]; H. Hijazi[a,b], J.-F. Paul[b], L. Gasnot[c], A.-C. Grégoire[a], A.-S. Mamede[b], L. Cantrel[a]

[a] Institut de Radioprotection et de Sûreté Nucléaire, Pôle Sûreté Nucléaire, CEN Cadarache, Saint Paul lez Durance F-13115, France

[b] Univ. Lille, CNRS, Centrale Lille, Univ. Artois, UMR 8181 - UCCS - Unité de Catalyse et Chimie du Solide, F-59000 Lille, France

[c] Univ. Lille, CNRS, UMR 8522 - PC2A - Physicochimie des Processus de Combustion et de l'Atmosphère, F-59000 Lille, France

Abstract

Iodine compounds that may be released in case of severe nuclear accident will have important radiotoxicity if they are disseminated in air. One of the most important iodine species is CsI that is deposited on the surfaces of the reactor coolant system. However, depending on the conditions, CsI can volatilize or react with oxidants to produce $I_{2(g)}$. Theoretical and experimental studies demonstrate that the oxidation of iodide depends on the temperature and in the presence of oxidants in the gas. It is also slightly influenced by the crystallinity of the CsI particles and the nature of the support. In case of a high temperature deposition, the iodine release started at temperature lower than 300°C. For the CsI vapour and aerosol depositions, the iodine is detected only at temperature above 450 °C and become very important above 550 °C.

Key words

Fission products, re-vaporization, severe nuclear accident, DFT calculations.

1. Introduction

In case of a severe accident (SA) occurring in a Pressurized Water Reactor (PWR), volatile radioactive fission products (FPs), such as caesium and iodine, are released from the degraded fuel. They are transported through the reactor coolant system (RCS) and the containment building and can be released into the environment via direct leakages of the nuclear containment and/or by the containment venting process in case of overpressure. As a result, these FPs can contribute to the radiological consequences for the population in the short term for iodine and the long-term for caesium.

In order to simulate an accidental scenario and predict the release of FPs, the ASTEC (Accident Source Term Evaluation Code) calculation code has been developed by the French Institute for Radiological Protection and Nuclear Safety (IRSN). In order to get predictive simulations[1], a comprehensive knowledge of all the phenomena occurring in a PWR during a severe accident situation is necessary. Considerable advances have been made in the field of understanding the behaviour of volatile FPs such as iodine after their release from the damaged core, thanks to experimental programs such as Phébus-FP [2] and other experimental works devoted to FP behaviour[3] and subsequent modelling works.

Nevertheless, some phenomena are not accounted for yet by the simulation tools and it is difficult to predict their outcome, mostly because of a lack of experimental and/or theoretical data. It is the case with the re-vaporization of FPs deposits from the surface of the RCS. FPs will form deposits on the surface of the RCS by different mechanisms, the most important of which are vapour condensation and thermophoresis as predicted by Hidaka *et al.* [4] and Maruyama *et al.* [5], as well as gravity deposition. The Phébus-FP experimental program has shown that Cs and I can significantly deposits in the RCS [6]. The main identified iodine compounds is CsI – resulting from condensation of CsI vapours in the 600-650°C temperature range (as expected from thermodynamic calculations and simulation with severe accident software as the ASTEC code [1]). Other condensed iodine form were identified too, but their nature could not be fully unravelled – they are expected to be metallic iodide of control rod material (Cd or Ag). Moreover, it was determined from Phébus tests, that Cs remobilization can reach up to 75% of the initial deposit in certain conditions [2]. More recently, in the aftermath of the Fukushima Daiichi accident, delayed releases for iodine and caesium have been detected several days after the accident [7] [8], and are believed to be related to the chemical re-vaporization of caesium and iodine containing deposits.

In the past several attempts have been made to understand the phenomenon of FPs remobilization. As a follow-up of the Phebus-FP tests, a series of research programs have been launched by several institutions. The studies focused mainly on the re-vaporization of caesium in a wide range of temperature and carrier gas conditions; iodine behaviour, for its part, was less studied. The studied precursor was mostly CsOH [8-12], less frequently CsI [10, 13, 14-16].

As for caesium, AEA-T [9] studied the re-vaporization of synthetic CsOH deposits in a flow reactor at temperatures reaching up to 1100°C, analysing the mass balance and surface interaction between caesium and the substrate made of 304 SS steel. Auvinen *et al.* [10] have studied the vaporization of CsOH and CsI powders from stainless steel crucibles. The samples were traced with radioactive Cs (^{134}Cs or ^{137}Cs), which allowed establishing a release kinetics thanks to γ-spectrometry measurements. The two studies used steam as carrier gas and it was established that the Cs re-vaporization starts at ≈500°C. Bottomley *et al.* [11] and Knebel *et al.* [12] performed online *γ*-spectrometry measurements of ^{137}Cs from deposits issued from the Phebus-FP tests (vapour deposition at temperatures up to 700°C), which are as realistic as possible. However the initial composition of the deposits, as well as the surface state of the stainless steel substrate is not well defined. The results show that in steam Cs is released starting from 550°C, whereas in air atmosphere the release occurs at a lower temperature, as low as 300°C.

The studies dealing with CsI were aimed at investigating conditions leading to CsI decomposition and subsequent gaseous iodine releases. Experiments performed by Kalilainen *et al.* [13] allowed a better understanding of the re-vaporized Cs and I distribution between gaseous and aerosol forms, thanks to the use of liquid scrubbers and filters adapted for each type of material. It was found that up to 27% of initial iodine content is released in gaseous form in an argon/steam atmosphere, and that it decreases with the introduction of hydrogen in the carrier gas. Shibazaki *et al.* [14] performed tests with CsI in steam and concluded that it starts re-vaporizing at ≈490°C and is released mainly as CsI. Berdonosov *et al.* [15] [16] conducted small-scale tests to further study the chemical nature of the released gaseous iodine. By heating CsI in air up to 1250°C, the formation of gaseous molecular iodine I_2 has been observed, the higher the temperature the larger the amount. Kulyukhin *et al.* [17] studied the hydrolysis of CsI in presence of molecular oxygen in the 630-1300°C range and the

formation of I_2 has been also confirmed, indirectly. However, some key parameters were not fully investigated in those studies. For instance, the FP deposit-substrate interaction was not always taken into account. Indeed, if some studies featured stainless steel substrates [10, 13] the initial surface state is not documented. Some studies featured even substrates not representative of the RCS (glass or platinum [14-16], alumina [10]). Secondly, the process of CsI deposition was not always examined as most of studies were performed with commercial CsI powder; CsI vapour and aerosol deposition were only considered in [13]. Finally, the influence of carrier gas composition and thermal conditions on re-vaporization were not fully investigated: most of studies considered steam or steam/hydrogen atmospheres which are more representative of early degradation phase during SA, whereas air was only considered in [14-16], but in the latter case, the thermal treatment (flash heating up to 1250°C) seems unrealistic regarding late phase SA conditions.

From the theoretical point of view, to the best of our knowledge, the revaporisation and the chemical reactivity of CsI aerosols had only been studied by H. Hijazi ([18]). The other theoretical studies in a nuclear frame focused on the gas reactivity of iodine species or on chemical stability/reactivity of caesium species ([19] [20] [21] [22] [23] [24] [25] [26] [27]. Severe accident simulations in the RCS are based on chemical equilibrium in gas phase thus ab initio computations were performed on the speciation at the equilibrium of the compound containing iodide or caesium. The gas inorganic chemistry involves mainly molecular iodine (I_2), monoatomic iodine radicals ($I^{\bullet}$) and iodine oxides (IO_x). The conversion between the species are fast and are favoured by oxidants such as nitrogen oxide and by visible light or radiation. The interaction with water occurs through the formation of hydrogen bonds and hydrogen transfer between acidic and radical species. The reactivity of caesium species in the gas phase has not been studied extensively. The reaction between CsO and H_2 have been investigated by Louis at al. [28]. Based on all these studies, it is possible to estimate the concentrations of some iodine and caesium species in the gas phase depending on the experimental conditions [29].

In conclusion, data on caesium and more particularly on gaseous iodine re-vaporization are too scarce and remain to be confirmed in more representative conditions to build an appropriate modelling.

The work presented here was aimed at fill in the gap in knowledge on CsI re-vaporization in conditions as representative as possible of a late phase of a SA scenario, in terms of: i/ substrate nature (pre-oxidized 304L and 316 L stainless steel which correspond to RCS steel composition) ii/ deposit generation (reproducing the different temperature deposition processes as in [13]: high temperature deposition, vapour condensation and finally aerosol impaction with realistic deposited amounts ~i.e. few mg/cm^2) iii/ re-vaporization thermal conditions (with heating up to 750 °C), iv/ presence of air (steam/air mixtures), since air is susceptible to penetrate in the RCS in case of an air-ingress accidental scenario[30]. We aimed at a better assessment of gaseous iodine release with the identification of re-vaporized species and their kinetics.

Preliminary results of the study have been published before [31], [32] and were focused mainly on the re-vaporization of CsI aerosol deposits in pure atmosphere (air or steam). This paper expands on the previous results and presents the re-vaporization of different types of CsI deposits in a mixed air/steam carrier gas as well as investigates the release kinetics for gaseous molecular iodine. Special attention was brought to the substrate nature, and its preparation in order to obtain a surface state

as similar as possible of RCS inner parts after several hours of oxidation in steam conditions [32] [33] at high temperature. The surfaces before and after deposit re-vaporization process were carefully determined by combining X-Ray Photoelectron Spectroscopy (XPS) and Time-of-Flight Secondary Ion Mass Spectrometry (ToF-SIMS). The release rate was monitored by thermogravimetric analysis (TGA) and the nature of released vapours was determined. Also, the release kinetics for molecular iodine has been studied by a novel spectroscopic technique, Incoherent Broadband Cavity Enhanced Absorption Spectroscopy (IBB-CEAS)[34].

Hereafter the article is composed of an experimental section which describes the equipment used and the analytical techniques employed. The following section presents the experimental results concerning the re-vaporization CsI deposits. Finally, a theoretical modelling of the experiments is done, in order to improve the understanding of the reaction mechanisms.

2. Materials and methods

The experimental study is based on a multistep approach including:

- Substrate pre-oxidation;
- CsI deposits generation;
- CsI deposits thermal treatment.

After each step the samples are characterized in order to establish the surface state of the substrate (XPS, ToF-SIMS), deposit quantity (ICP-MS), mass balance for caesium and iodine after re-vaporization (ICP-MS, TGA, UV-Visible spectroscopy).

2.1. Substrate pre-oxidation

304L stainless steel coupons (8×15×2 mm), whose composition is presented in Table 1, underwent a thermal treatment in a controlled atmosphere in a flow reactor to reproduce as close as possible the surface state of the RCS inner part in SA conditions. The thermal treatment consisted in exposing the coupons to a flow of argon/steam (% vol. 50/50) at 750 °C during 24 h. The heating rate was 5°C/min and steam was injected at 150 °C. The total gas flow rate was fixed at 1 L_n/min[1] at standard conditions. 316L foils (100×500×0.075 mm, see composition in Table 1) were pre-oxidized in the same thermal conditions and process gas composition, except that the total gas flow was 4 L_n/min at standard conditions. In both case, the carrier gas flow was laminar and steam proportion in the flow (50%) is large enough to allow equivalent oxidation conditions of the stainless steel surfaces.

Table 1. General composition (wt. %) of the 304L and 316L stainless steels ([32])

	C	Cr	Fe	Mn	Mo	Ni	Si	Other
304L	0.03	18.0-20.0	base	2.0		8.0-12.0	1.0	P,S<0.045
316L	0.03	16.0-18.0	base	2.0	2.0-3.0	10.0-14.0	0.75	P,S<0.025

2.2. CsI deposits generation

[1] The gas flow rates are given for the reference conditions: 273 K, 101325 Pa and are thus noted L_n/min

In this study three types of CsI deposits were considered: aerosols impaction at room temperature by Room temperature (RT) aerosol impaction, high-temperature vapour deposition/condensation and temperature aerosol deposition.

The CsI impacted aerosols were obtained following the procedure described by Obada *et al.* [33] which consists in nebulizing a concentrated CsI aqueous solution. The obtained wet aerosols are then dried in a strong argon flow (10 L/min) and afterwards impacted on the pre-oxidized 304L coupons placed in an exposition chamber (8 coupons per batch).

The high-temperature CsI deposits were generated using a high-temperature furnace. The thermal profile of the heated alumina tube is bell-shaped, with a 5 cm isotherm zone at the centre. An alumina crucible (5 cm) containing CsI powder (Acros Organics, 99.9%) was placed inside a 1 m long alumina tube (30 mm inner diameter), inserted in the furnace. The crucible was placed in the isothermal zone. Downstream the alumina tube wall was lined by a 316L pre-oxidized foil. The crucible was heated up to 750°C (5°C/min rate) and the temperature was maintained at 750°C for 6 hours. The carrier gas was a mixture of argon and steam (% vol. 20/80) at total gas flow of 0.62 L_n/min. The 316L foil was placed in a strong thermal gradient as such vaporized CsI was transported by the carrier gas and was deposited along the pre-oxidized 316L foil in a wide temperature range (from 750 to 150°C)_ covering thus all deposition processes from a high temperature vapour deposition (above 620°C), vapour condensation (between 620 and 400°C) and aerosol deposition (below 440°C). Downstream of the alumina tube was a series of two liquid scrubbers containing an alkaline solution (NaOH 0.1M) dedicated for steam condensation and trapping any non-deposited material. The line was terminated by an integral filter. After the test, the 316L foil is recovered and divided into several sections (~2-3 cm long and 1-2 cm large) based on a visual inspection of the deposit.

The deposited mass is determined after leaching one of the 304L coupons (wet deposition) and a selection of small 316L samples, cut from the foil (high temperature deposit generation) in selected area, in alkaline media (NaOH 0.1 M) for I and Cs recovery in solution followed by elemental I and Cs determination by Inductively Coupled Plasma – Mass Spectrometry (ICP MS –Varian 810 MS).

CsI deposits thermal treatment

The re-vaporization of CsI deposits from pre-oxidized stainless steel surfaces were carried out in a thermogravimetric analysis (TGA) device as described by Obada *et al.* [31]. Given the TGA furnace geometrical constraints (inner diameter of less than 1 cm), only the 304L coupons could be thermally treated in this device. The thermal treatment consisted in heating the samples up to 750°C (except for some tests, where samples were heated up to 970°C or 550°C only) at a rate of 5°C/min and hold for 1 hour, before cooling down by natural convection. The rate of the heating ramp is a compromise between chemical equilibrium conditions and test duration (2-3 hours) [35]. During the thermal cycle, the sample is swept by a low carrier gas flow either composed of synthetic air (30 mL_n/min) or air/argon/steam mixtures (air/steam mixture featuring a total flow rate of 30 mL_n/min; argon flow rate set at 70 mL_n/min). Air/steam mixtures were injected at temperature above 150°C and switched off during the cooling phase (below 400°C).

The main outcome of the TGA tests is the onset temperature of the mass loss linked to the start of the re-vaporization process. The overall mass change (loss) cannot be considered as a measure of CsI

re-vaporization as the oxidation of the substrate during the thermal treatment may counterbalance the mass loss linked to re-vaporization. On the more, the inner alumina liner of the TGA device presents an important reduction in diameter (from 1 cm to 0.4 cm (Obada [2017]) just downstream of the sample, probably inducing at its vicinity some perturbation in the fluid flow which may enhance deposit retention on the sample.

To complement the results obtained by TGA, the RIGolo (**R**e-vaporization of **I**odine in **G**aseous form and "picc**olo**"="small" in Italian) experimental device has been developed with a double purpose:

- Establish the nature and quantity of released iodine-containing species;
- Determine the release kinetics for gaseous molecular iodine.

It is an open flow reactor (Figure 1) composed of a tubular furnace (WATLOW ceramic heater CF-964255, 15 cm) in which an alumina tube (45 cm long, 20 mm inner diameter) is inserted. The sample is placed at the centre of the furnace and the carrier gas is fed up at the inlet of the test line. The vaporized vapour and/or generated aerosols from the heated sample are transported by the carrier gas to the line outlet. Based on the type of information searched in the experiment, the downstream part of the RIGolo device has two configurations: "integral measurement" for determining the nature and quantity of released iodine-containing species and "online measurement" for establishing the gaseous I_2 release kinetics.

The "integral measurement" configuration is described by Obada *et al.* [31] and consists in connecting the alumina tube outlet to a series of selective liquid scrubbers, containing a mix of toluene/acidic water. It has been shown that in these conditions molecular iodine will be selectively trapped in the organic phase, while inorganic iodine compounds (CsI, HI) will be trapped in the aqueous phase [36] [37]. Since the detection limit of I_2 in toluene by UV-Visible spectroscopy is between $2x10^{-8}$ and $6x10^{-7}$ mol/L (for the absorption wavelengths of 309 nm and 496 nm respectively), it is necessary to accumulate I_2 over a long period of time (2 h), hence the experiment was called "integral".

The "online measurement" configuration consists in connecting the alumina tube outlet to an Incoherent Broadband Cavity Enhanced Absorption Spectroscopy (IBB-CEAS) device dedicated to monitor online the gaseous molecular iodine concentration, transported up to the optical cell, by absorption spectroscopy in the 510-570 nm range [38] [34]. In this case the re-vaporization products (gaseous species, aerosols) are diluted in an argon flow before being injected in the optical cell. The technique has a low detection limit (1 ppb volumic in the gas phase) and a good temporal resolution (10 s), which makes possible a kinetic study in our experimental conditions (1-2 mg of iodine re-vaporized for ≈1 h in a 200 mL_n/min gas flow).

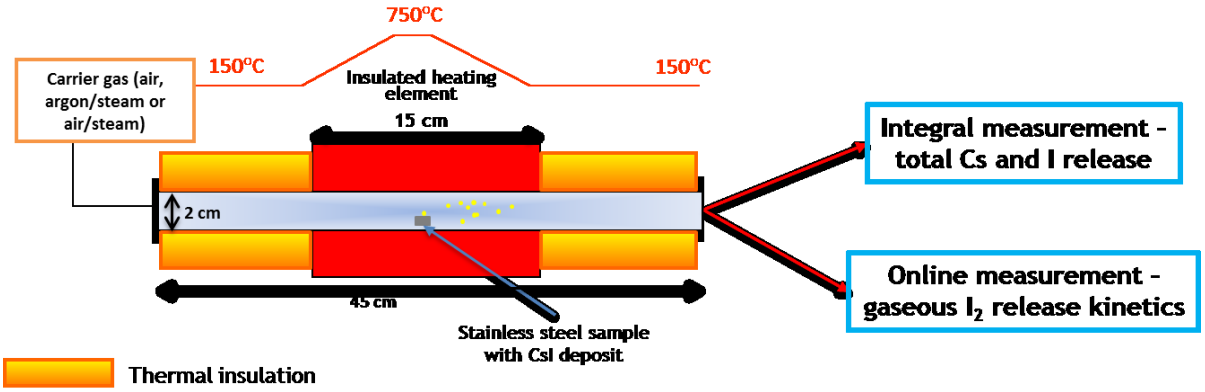

Figure 1. General design of the RIGolo experimental device

The thermal treatment in the RIGolo device is similar to the one applied in the TGA device: heating up to 750°C (rate 5°C/min) and hold for 1 hour, before cooling by natural convection. The carrier gas during the tests was either air (53 mL_n/min) or a mixture of air/steam (200 mL_n/min) of variable composition. The gas flow rates have been adjusted to the new alumina tube inner diameter, in order to have the same gas velocity above the sample as in the TGA tests.

2.3. Post-test analysis

2.3.1. Elemental mass balance determination

After each test, the entire facility, including the stainless steel and gold coupons, was leached in alkaline media for iodine and caesium deposits recovery and elemental determination. As in [31], the solutions were analysed by ICP-MS for elemental quantification with an uncertainty of +/- 8% (at 95 % confidence level). The organic phase of the liquid scrubbers has been also recovered and analysed by UV-Visible spectroscopy for quantification of I_2 in toluene, which was performed with an Agilent Cary 8454 spectrometer at 309 nm and 496 nm with an uncertainty of +/- 6% (at 95 % confidence level).

2.3.2. Surface Characterization Techniques

The sample surface was characterized by combination of X-ray Photoelectron Spectroscopy (XPS) and Time-of-Flight Secondary Ion Mass Spectrometry (ToF-SIMS). XPS provides chemical composition of less than 10 nm depth scale of the surface while the ToF-SIMS was used in depth profiling mode to reach composition up to several micrometres in depth. The morphology of the surface before and after re-vaporization was investigated by Scanning Electron Microscopy (SEM).

XPS measurements were carried out on a Kratos AXIS Ultra^{DLD} spectrometer equipped with a monochromatic Al Kα source (1486.6 eV). Calibration was done by using the C 1s component of adventitious at BE (binding energy) = 285.0 eV. Binding energy value uncertainty is +/-0.1 eV and uncertainty on quantitative elemental analysis is +/- 10%.

ToF-SIMS analyses were carried out using a ToF-SIMS 5 instrument (ION-TOF GmbH). Pulsed Bi^+ primary ions have been used for analysis (25 keV, ≈1 pA) and O_2^+ for sputtering (2 keV, ≈500 nA). Given the sputter parameters, estimated sputter speed is 1.6 nm/s. Mass spectra were recorded in positive (for each sample) and negative for one sample polarity from an analysis area of 100µm x

100µm centred into a 300µm x 300µm sputtered area. Charging effects, due to analysis and erosion ion beam, were compensated using low energy electrons (20 eV).

Scanning Electron Microscopy (SEM) images were obtained using a LEO-435 VP microscope. A 20 kV accelerating voltage was used giving an interaction depth above 2.5 µm[3].

2.3.3. IBB-CEAS signal interpretation and presentation

The IBB-CEAS configuration and characteristics are extensively discussed in [38] and [34]. It is based on the I_2 fine resolved spectrum in the 510-570 nm spectral range owing to the numerous rovibronic transitions in the I_2 B←X electronic absorption spectrum [38]. The light source is a LED emitting in the 480-580 nm and the detector is a CCD camera (Andor iDus).

As explained by Bahrini *et al.* [38] and Johansson *et al.* [34], the I_2 spectra registered by the CCD detector require mathematical processing in order to separate the spectral contribution of gaseous molecular iodine from the continuous component of the spectra. Moreover, for practical reasons [38], a calibrated source of I_2 is analysed by the IBB-CEAS at the beginning of each experiment. Iodine concentration in the sample is then displayed as the adimensional N_{rel} value which is the ratio of I_2 sample concentration to the calibration source concentration. Absolute concentration in the samples requires to be adjusted for the sampling, calibration and dilution flow rates. In our case, as the main objective is to determine the release kinetic, it was decided to stay with relative concentration. For comparison purpose, the kinetic curves were rescaled based on the overall fractional release of molecular iodine, whenever possible (data from integral RIGolo experiments). Hereafter the figures displaying I_2 release kinetics present the rescaled N_{rel} evolution as a function of time and temperature.

2.3.4. DFT Calculations

All DFT (density functional theory) calculations were carried out with VASP (Vienna Ab initio Simulation Package [39] [40] [41]**.** Plane waves are used to describe the wave functions and the PAW (Projector Augmented Wave) [42] method for electron-ion interactions. The energy is calculated using GGA as parametrized by Perdew et al., [43] and with a Methfessel-Paxton[44] smearing parameter sigma set to 0.1 eV. The Kohn–Sham equations are solved self-consistently until the energy difference between two successive steps is lower than 10^{-5} eV. The atomic positions were optimized without symmetry constraints until the forces being less than 0.03 eV/Å. The electron configurations [Xe] 6s1, [Kr] 4d10 5s2 5p5, [He] 2s2 2p4 and 1s1 were used for caesium, iodine, oxygen and hydrogen respectively. The cut of energy was set to 450 eV and 3x3x1 or larger K-point meshes [45] have been used for all the surface calculations (distance between K point smaller than 0.035$Å^{-1}$). Van der Waals interactions are included in the calculation through the TSHI formalism[46] that take into account the charges on the atoms.

The adsorption energy (E_{ads}) is defined as the opposite of the adsorption reaction energy. A positive adsorption energy is associated to an exothermic adsorption.

$$A_{(g)} + \text{Surface} = \text{A-Surface} \qquad E_{ads} = E(A_{(g)}) + E(\text{Surface}) - E(\text{A-Surface}).$$

3. Experimental matrix

The first tests concerning the re-vaporization of CsI aerosols (Room temperature aerosol impaction) from pre-oxidized 304L or 316L substrate in presence of argon/steam have shown an integral release of Cs and I [31]. As such these test conditions will serve as reference. The goal of this research was to assess gaseous iodine release during re-vaporization of CsI deposits, through small-scale analytical tests.

Stainless steels of different grades (304L or 316L) were used to represent the inner surface of the RCS in general. The coupons were pretreated (pre-oxidation at 750°C in steam conditions) so as to feature a surface state representative of the RCS in case of a SA. As reported in [32], the structure of surface oxide is similar for both stainless steels grades and has no influence on the CsI re-vaporization behaviour. In the case of 316L foils, oxide structure is slightly different, presenting an outer Fe-rich layer (as opposed to a Mn-rich layer) and an inner Cr-rich layer. Nevertheless, taking into account the thickness of the deposit (estimated to be in the range of 2-7 µm for 1-3 mg/cm^2 for deposited CsI), we expected a low contribution of deposit/surface interaction on re-vaporized species. Indeed, for such thick deposits, the fraction of CsI in contact with the substrate surface is low.

Except for one test, the same thermal cycle was applied: heating at 5°C/min up to 750°C. This final temperature is high enough to be able to catch every release events concerning CsI re-vaporization and remains within the expected temperature range which could prevail in the RCS during a late SA phase.

The study was focused on the two main following parameters (see table 2):

- The CsI deposition process, to be able to reproduce the different deposition zones in the RCS: RT temperature aerosol impaction (simulating CsI deposition in the cold leg of the RCS), high temperature vapour deposition (above 620°C, simulating a deposition in the hot leg of the RCS and SG inlet), vapour condensation (620-400°C, simulating SG deposition) and temperature aerosol deposition (around 400°C, SG deposition).
- The atmosphere composition featuring either air, air/steam mixtures and argon/steam. Air and steam atmospheres are not representative of SA scenario but may help in understanding the CsI re-vaporization behaviour and gaseous iodine production. Realistic atmospheres are mixture of air/steam with a low air content. Re-vaporization of CsI aerosols (RT aerosol impaction) on 304L coupons featured the largest atmosphere compositions (5 different compositions as reported in table 2, from pure air contents to argon/steam). Tests were performed in both TGA and RIGolo devices. Based on the results of this test series, the number of tested atmospheres has been reduced for the CsI vapour deposition and vapour condensation: one test in steam, one in air and one in a 20/80 air/steam atmosphere. Finally, for the deposit obtained by temperature aerosol deposition (400 °C), only the pure air and steam atmospheres have been retained for the re-vaporization tests, to check for consistency with CsI aerosol impaction at room temperature. The tests have been performed in the RIGolo device only, as the 316L foil samples were not suited for the TGA device (see table2).

Two complementary tests were performed:

On test with an inert substrate to assess the contribution of deposit/surface interaction in terms of nature of re-vaporized species (especially for iodine). CsI aerosols were deposited on gold coupons by the room temperature aerosol impaction process. Tests conditions featured air atmosphere and a thermal cycle (5°C/min up to 750°C) similar to conditions 1. Tests were performed in both devices (TGA and RIGolo) to allow a complete comparison with condition 1, table 2.

One test with a lower final test temperature (550°C), dedicated to the observation of iodine re-vaporization kinetics at low temperature. This test was conducted with initial CsI RT aerosol deposits on a stainless steel coupon ad a mixed steam/air atmosphere was applied (instead of pure air) to be more representative of a reactor case. This test was performed in the RIGolo device in the I_2 on-line monitoring configuration. The sample was initially heated up to 420°C in argon (rate 5°C/min), then the carrier gas was switched for a mixture of air/steam (% vol. 50/50). After that the sample was heated up to 550°C (rate 5°C/min) and held for 4 h before cooling by natural convection. The upper limit for temperature was chosen based on the results of Bottomley *et al.* [11], where it has been observed that Cs re-vaporization is much slower and less significant after 750-800°C.

Table 2. CsI re-vaporization - Experimental matrix for test performed with thermal cycle up to 750°C at 5°C/min.

Substrate	Deposition process	Re-vaporization carrier gas (% vol)	Experiment type (repeat)			Condition n°
			Integral[1]	Kinetic[2]	TGA[3]	
Pre-oxidized 304L	Aerosols impaction at room temperature	Air (100%)	x [31] (3)	x	x [31]	1
		Air/steam (50/50)	x	x		2
		Air/steam (20/80)	X (2)	x	x	3
		Air/steam (3/97)	x	x	x	4
		Argon/steam (50/50)	x[29]		x [29]	5
Pre-oxidized 316L	High-temperature vapour deposition (720-620°C)	Air (100%)	x	x		6
		Air/steam (20/80)	x			7
		Argon/steam (50/50)	x			8
	Vapour condensation (620-440°C)	Air (100%)	X (2)	x		9
		Air/steam (20/80)	X	x		10
		Argon/steam (50/50)	X			11
	Aerosols deposits (< 400°C)	Air (100%)	X			12
		Argon/steam (50/50)	x			13
Gold (Au)	RT aerosol impaction	Air (100%)	x	x	x	14

[1] RIGolo with biphasic liquid scrubbers

[2] RIGolo coupled to the IBB-CEAS

[3] Thermogravimetric analysis

4. Results

4.1. Deposit characterization

After the pre-oxidation of 304L and 316L stainless steel coupons and foil, CsI is deposited as described in section 2.2. Afterwards the size and the morphology of the deposits are characterized by SEM and the amount of deposited CsI is determined by ICP-MS after lixiviation.

The CsI aerosols deposits obtained by impaction at room temperature have been described by Obada *et al.* [33]. SEM analysis has revealed the presence of particles with irregular shapes and particle agglomerates with sizes from 5 to 20 µm. After several weeks, the particles also appear to hydrate, given the hygroscopic nature of CsI [47]. ICP-MS analysis has revealed similar CsI quantity among all

the 304L coupons of the same batch, with values ranging from 0.8 to 4.2 mg/cm^2 of CsI from one experiment to another.

The Cs and I deposits obtained at high temperature, on the other hand, exhibit different sizes and morphologies based on the deposition temperature. For instance, in the 720-620°C temperature range, SEM analysis has revealed an amorphous deposit, homogeneously spread across the entire surface of the 316L foil (Figure 2a) – corresponding to the deposition of liquid droplets. The average amount of caesium and iodine per surface unit in this temperature range is about 2.9 mg/cm^2, as determined by ICP-MS analysis. Also, the Cs/I mass ratio of 0.94 is consistent with to the theoretical value (1.05) taking into account uncertainties measurement, which strongly suggests that caesium and iodine were deposited as CsI. In the 620-440°C temperature range, the deposit is composed of polyhedrons that range between 10 and 30 µm in size, as well as acicular particles with lateral dendrites that reach several hundred microns in size (Figure 2b). The deposit in this temperature range is the most important in terms of quantity, up to 8.3 mg/cm^2, and the Cs/I mass ratio (0.96) suggests that the chemical species is CsI. Below 440°C, the deposit consists of spherical particles that reach up to 4 µm in diameter (not presented here). The amount of deposit decreases progressively from 4.3 mg/cm^2 at 440°C to 0.7 mg/cm^2 at 150°C. Given the Cs/I mass ratio (0.89-0.99), it is highly likely that the deposit is composed of CsI.

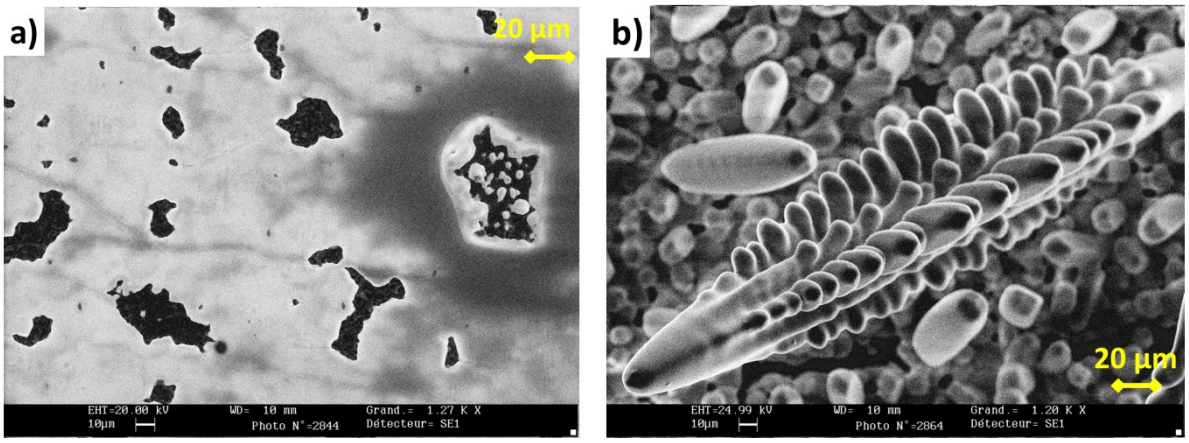

Figure 2. SEM images of high-temperature CsI deposit on pre-oxidized 316L foil: a) between 720-620°C and b) between 620-440°C.

4.2. Re-vaporization: identification of released and residual species and release kinetics

In this chapter are presented the results of RIGolo and TGA tests in different conditions (Table 2) as well as the results of the kinetics tests. Since the goal is to investigate the separate effect of different parameters, the results are presented following the listed parameters: carrier gas composition, deposition process, substrate nature (stainless steel vs gold) and finally low temperature re-vaporization. Here the main trends will be discussed depending on the test parameters. Variability in test results may occur for equivalent test conditions (and for repeats) due to inhomogenities of CsI deposits.

4.2.1. Influence of carrier gas composition: air vs. mixed air/steam (conditions 1 to 5)

As previously reported [31] [33], the carrier gas composition during the re-vaporization phase is one of the key parameters regarding the nature of re-vaporized and residual species. As such, in an

argon/steam carrier gas, caesium and iodine are released integrally from the surface of stainless steel coupons (condition 5). The absence of gaseous iodine species at the line outlet and Cs/I ratios measured downstream of the steel coupon close to ~ 1.1 (main line data), suggest a re-vaporization as CsI only [31].

With the addition of air in the carrier gas (in increasing amounts following conditions 4, 3, 2 up to pure air, condition 1), we can observe that the overall fraction of released molecular iodine (RIGolo test in integral configuration) is roughly the same (~ 23-33% of total iodine) as soon as air is present in the gas phase, except for pure air conditions featuring much higher gaseous iodine releases (up 75% of total iodine amount). Indeed, oxygen is always present in sufficient amount to react with iodine taking into account the oxygen flow (from ~0.02 up to 0.7 mg/s), the test duration (2 hours of heating and one hour at 750°C) and the initial iodine mass (1-2 mg) – so that the role of oxygen is expected to be the same in all the cases as soon as it is present (see section 5 for theoretical part). In pure air, TGA tests have shown that the release starts at 420°C on average, releases seems to be delayed as soon as steam is present with onset temperatures in the 450-470°C range. These observations (lower gaseous iodine releases and higher re-vaporization onset temperature) in air/steam conditions compared to pure air condition may be owed to possible limiting effects of steam which are not yet understood.

Concerning the residue (RIGolo tests in integral configuration), the ICP-MS analysis of the leaching solutions of the stainless steel coupons has consistently revealed the absence of iodine, which implies its total re-vaporization, and the presence of a residual amount of caesium. In pure air (Table 3, condition n°1), Cs retention amounts up to 10 % of the total measured amount at the end of the test. The ICP-MS analysis of the alumina tube leachate shows a Cs/I mass ratio in between ≈ 5-11. This feature indicates that beside CsI, Cs is mainly deposited in other chemical forms – expected to be CsO as this species is the most stable from a thermodynamic point of view in the absence of steam. In air/steam, Cs retention on the coupon represents up to 9% of total Cs collected mass (Table 3, conditions n°2 & 3). The integral experiment in conditions n°4, which featured the smallest ratio of air to steam (% vol. 3/97), has resulted in a residual amount of Cs of only 1.5%. The Cs/I mass ratio in the alumina tube does not vary a lot when considering all the mixed air steam conditions (1.4-1.6). This value is still above the Cs/I mass ratio of CsI (1.05) and support the hypothesis that beside CsI, other Cs compounds may have deposited in the main line (though in a lesser extent compared to pure air condition). In presence of steam, the other expected Cs compound is CsOH.

A detailed surface characterization by XPS and ToF-SIMS of 304L samples after re-vaporization in air or argon/steam has been discussed by Obada *et al.* [33]. The same process has been applied to the 304L samples obtained after re-vaporization in air/steam atmosphere and the results show evidence of the formation of mixed Cs-Cr oxides, specifically Cs_2CrO_4 and $Cs_2Cr_2O_7$. This observation is supported by XPS analysis which revealed the presence of two chemical forms of chromium: Cr(III) and Cr(VI) oxides. Also, ToF-SIMS analysis has revealed the presence of secondary ion clusters $Cs_2CrO_3^+$ and $Cs_2Cr_2O_9H^+$, which is a strong indication that the said oxides have been formed during the re-vaporization process. These results demonstrate that the nature of the support affect the behaviour of residual Cs+ but not that the same support participate to the iodine oxidation but that in oxidizing condition, the chromium of the support can react with the air[48].

This test series (conditions 1 to 5) was complemented by RIGolo tests performed with the on-line configuration in order to monitor I_{2g} release during the thermal treatment. Based on TGA tests results (no release event below 400°C) , the I_2 release kinetics was monitored from ~ 330°C on.

A first test has been performed in an argon/steam atmosphere (condition 5), serving as reference (Figure 3, red curve). There is no signal increase up to 640°C, indicating the lack of gaseous I_2. The weak signal detected in the 640-680°C temperature range and interpreted as $N_{rel} \neq 0$ is nevertheless not representative of any I_2 release kinetics. Indeed, the raw spectra in this temperature range lack the fine structure of the I_2 spectrum [38] [34] and thus the signal is attributed to the light extinction due to the presence of aerosols (probably CsI) transported up to the optical cell. This online measurement experiment with a sensitive technique confirmed the absence of gaseous molecular iodine released in steam conditions.

In pure air (Table 2, condition 1), I_2 release starts at approx. 440°C, which is coherent with the TGA tests, and occurs in two steps (Figure 3, blue curve):

1) Between ≈440-550°C a first slow and low release is observed ;
2) Above 550°C the majority of iodine is rapidly released (exponentially). Reproducibility tests have been performed in these conditions and the results were similar.

Further on, the re-vaporization tests in air/steam atmosphere (Table 2, conditions 2, 3 and 4) showed that I_2 release is initiated at a higher temperature, ≈480-500°C (Figure 4), compared to air re-vaporization, which is coherent to the TGA results of similar tests. While the release of I_2 in two steps is still noticeable for the % vol. 50/50 (condition 2), it is less pronounced for the other two carrier gas compositions (conditions 3 and 4). It is also interesting to note that the release curves present "spikes" (above ≈520°C), which resemble those in the case of argon/steam re-vaporization. This suggests the presence of a larger amount of aerosols, which in turn prevent a reliable measurement of I_2.

461

462 **Table 3. Summary table of main experimental results.**

Substrate	CsI deposit	Re-vaporization carrier gas (% vol)	Main results					Cond n°
			Temp. of release initiation (°C)[4]	I_2 released[1,2]	Cs residual [1,3]	I residual [1,3]	Cs/I line1	
Pre-oxidized 304L	Aerosols impaction at room temperature	Air (100%)	420	50-75 %	<10%	<1%	5-11	1
		Air/steam (50/50)	460	26%	6.5%	< l.d.	1.5	2
		Air/steam (20/80)	470	23-33%	7-9%	< l.d.	1.6	3
		Air/steam (3/97)	450	26%	2%	< l.d.	1.4	4
		Argon/steam (70/30)	480	0%	3.4%	< l.d.	1.1	5[29]
Pre-oxidized 316L	High-temperature vapour deposition (720-620°C)	Air (100%)		53%	3.4%	< l.d.	10	6
		Air/steam (20/80)		13%	9.7%	8.6%	1.6	7
		Argon/steam (70/30)		0%	1.9%	< l.d.	3.8	8
	Vapour condensation (620-440°C)	Air (100%)		7-15%	2.4-4.5%	<1%	1.3	9
		Air/steam (20/80)		12%	2.0%	<1%	1.1	10
		Argon/steam (70/30)		0%	0.5%	0.6%	3.1	11
	Aerosols deposits (< 400°C)	Air (100%)		45%	2.4%	< l.d.	12	12
		Argon/steam (70/30)		0%	2.9%	1.0%	1.2	13
Gold (Au)	Aerosols Impaction (RT)	Air (100%)		28%	0.4%	< l.d.	1.6	14

463

[1]wt% wrt the total collected Cs and I at the end of test [2]As measured by UV-Visible spectroscopy
[3]As measured by ICP-MS [4]As measured by TGA

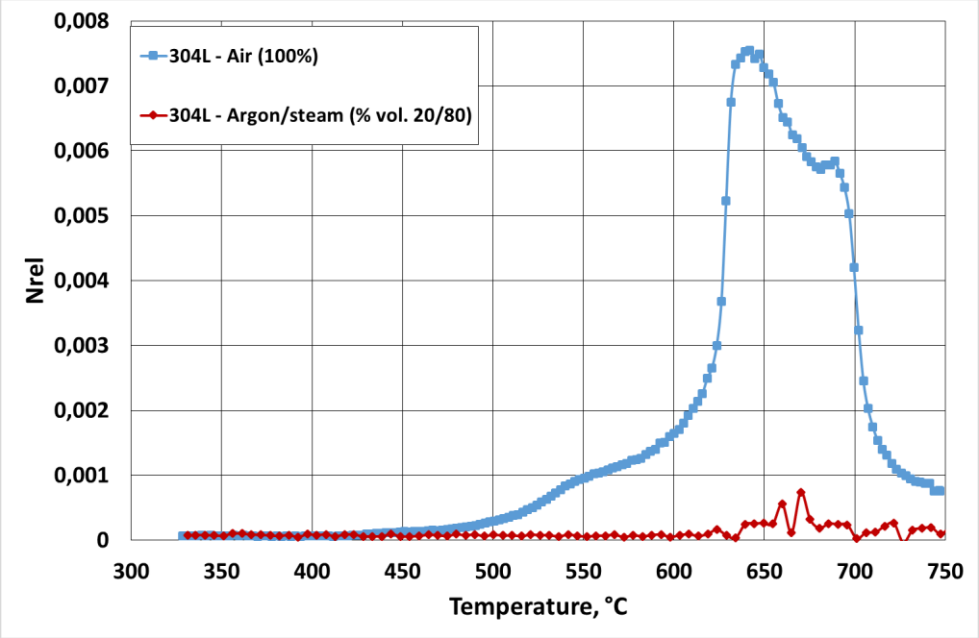

Figure 3. Release and transport kinetics of I_2 during re-vaporization of CsI aerosols (RT aerosol impaction) with a heating rate of 5°C/min up to 750°C; blue curve : pure air with a flow rate of 53 mL_n/min (condition 1) ; red curve : argon/steam (70/30) with flow rate of 200 mL_n/min (condition 5).

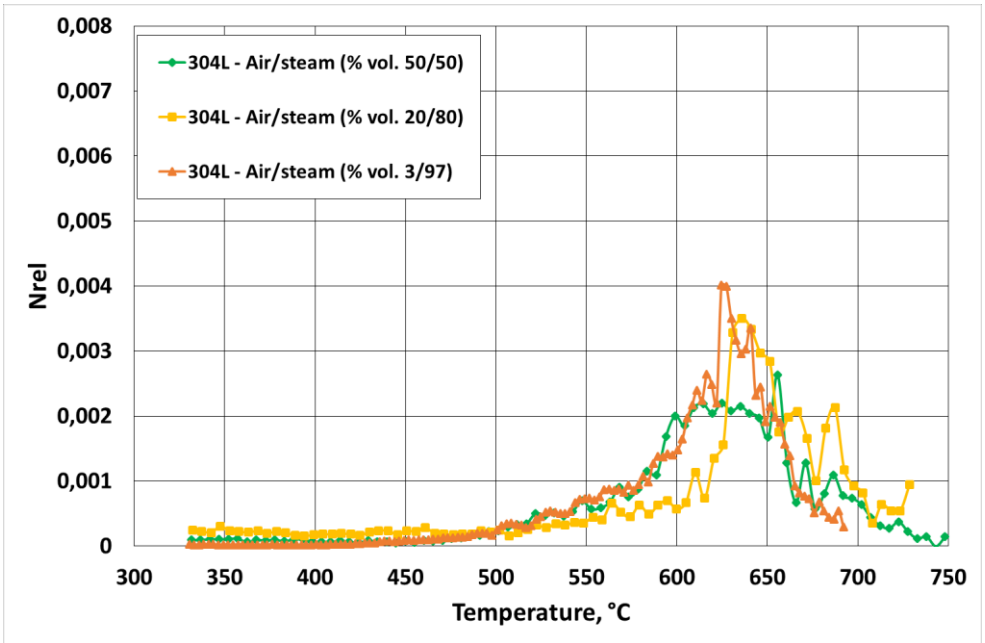

Figure 4. Release and transport kinetics of I_2 during re-vaporization of CsI aerosols (RT aerosol impaction) with a heating rate of 5°C/min up to 750°C. green curve: air/steam % vol. 50/50 (condition 2); yellow curve :, air/steam % vol. 20/80 (condition 3); orange curve : air/steam % vol. 3/97 (condition 4). Gas flow: 200 mL_n/min for all conditions.

4.2.2. Influence of CsI deposition process: high-temperature (conditions 6-13) vs. aerosol impaction at room temperature

As a general rule, the re-vaporization of CsI deposits obtained by different routes follows the same trend if the same experimental conditions are applied.

Compared to RT aerosol impaction, CsI aerosols deposited in the 400-150°C temperature range present a similar re-vaporization behaviour with atmosphere composition (table 3, air and argon/steam conditions only): similar gaseous iodine releases and overall deposition trends were observed for the RIGolo integral tests. It is thus assumed that CsI re-vaporization behaviour is very close when considering deposited aerosols.

For the two other deposition routes (high temperature vapour deposition 720-620°C and vapour condensation 620-440°C), re-vaporization in argon/steam (conditions 8 and 11) didn't lead to the release of I_2; those results are comparable to the re-vaporization of CsI aerosols (conditions 5 and 12). Nevertheless, the Cs/I mass ratio in the RIGolo line is much higher (3.8 and 3.1 for conditions 8 and 11 respectively) compared to condition 5 (1.1). This observation indicates that besides CsI, other species can be involved during steam re-vaporization of such CsI deposits. CsOH is a possible candidate for the other Cs compounds, the iodine transported species could not be clearly identified.

Re-vaporization in air of the high-temperature deposits (condition n°6) and the aerosols deposits in has resulted in the release of 53% of iodine as I_2. The ICP-MS analysis of the alumina tube leachate shows a Cs/I mass ratio ~ 10. Both results are consistent with the re-vaporization behaviour of CsI aerosols as described in section 4.2.1. Only one mixed air/steam carrier gas composition (% vol. 20/80) was tested with the high-temperature (720-620°C, condition 7) and vapour condensation (620-440°C, condition 10) deposits. The results show that 12-13% of iodine is released as I_2 and that the Cs/I ≈ 1.1 – 1.6 in the alumina tube, which is again consistent with the results presented in section 4.2.1. However, there was a noticeable difference in the amount of released molecular iodine for condition 9. The re-vaporization in pure air of a CsI deposit obtained by vapour condensation (620-440°C) resulted in the release of only 7-15% of I_2, which is much lower when compared to the amount of released I_2 in other experiments in the same re-vaporization conditions. The residual amount of Cs on the steel coupon is 2.4 – 4.5 % and the Cs/I ≈ 1.3 in the alumina tube, suggesting the re-vaporization of Cs as several different species. The possible reasons, which may be linked to the organized crystalline structure of the deposit, are discussed further.

Surface characterizations by XPS and ToF-SIMS have been performed on the 316L foils after CsI re-vaporization of high temperature deposits and condensed vapour (as displayed in figure 6). The presence of the mixed Cs-Cr-O compounds described above (see section 4.2.1) is confirmed (figure 6b, depth profiles in negative polarity), as soon as air is present in the carrier gas. Also, in both cases, the Cs depth profile indicates that Cs had migrated in the oxide layer during the thermal treatment – or that the oxide layer may have growth up to the CsI deposit. Indeed the Cs_2^+ and Cs_2I^+ signals are very low at the surface and in the first oxide layer (composed of Fe and Mn) and increase strongly in the second Cr-Mn oxide layer (figure 6, depth profile in positive polarity). Migration of CsI inside the oxide layer may explain the significantly more important residual mass of Cs (9.7%) and I (8.6%) observed on the 316L foil after re-vaporization of high-temperature vapour deposit in steam/air (table 3, condition 7) .

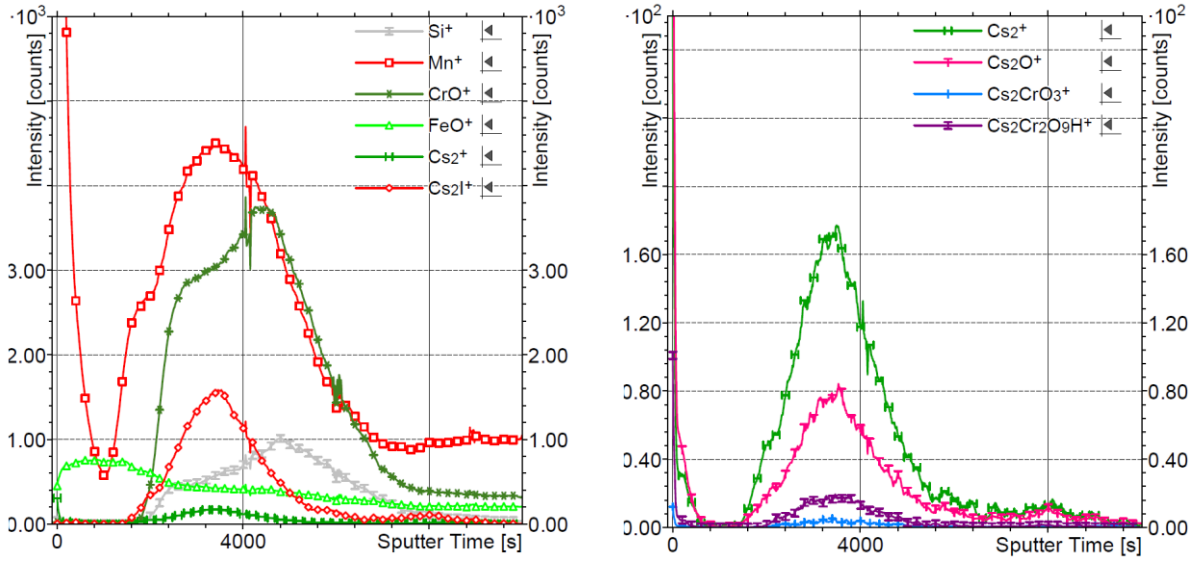

Figure 5. TOF-SIMS profile of CsI vapour condensation deposition 316L pre-oxidized foil and re-vaporized in air/steam atmosphere (condition 10, table 3). Secondary ions in positive polarity a) major fragments and b) minor fragments.

Based on the results of the integral tests, online measurement tests have been performed with CsI high-temperature (720-620°C) and vapour condensation (620-440°C) deposits with the same thermal cycle as for conditions 6 and 9. The carrier gas was pure air. The I_2 release kinetics from CsI deposits obtained by vapour condensation (condition n°9) presents a similar pattern as from CsI deposits obtained by RT aerosol impaction (condition n°1) (Figure 6). The process occurred in two steps: 1) a slow and low release between ≈350-500°C, and 2) a more rapid re-vaporization above 500°C, which results in the total release of iodine from the surface of the pre-oxidized 316L foil.

The kinetic study of I_2 release in case of a high-temperature CsI deposit (720-620°C), on the contrary, has highlighted a new phenomenon. While the cumulated amount of released I_2 is consistent with the release observed in condition 1 (RT aerosol impaction), the I_2 release and transport kinetics is slightly different (Figure 5). There is a two-step molecular iodine release between ≈400-550°C (slow) and above 550°C (rapid), which is consistent with previous results. However, there is an additional release peak between ≈200-350°C, which has been reproduced in another test, hinting at a different re-vaporization process, probably linked to the nature of the deposit in this temperature range (720-620°C). This new release mechanism may be owed to the CsI deposition temperature which resulted in a non-uniform amorphous like layer of deposits (see section 4.1) which is quite different to aerosol impaction [29] so that one can expect strong evolution at the molecular level too (for instance in the structure of the CsI outermost surface), inducing differences in the reaction mechanism – as will be seen with the DFT calculations (section 5).

The kinetic test results have shown the absence of any release below 200°C, hence the I_2 release kinetics for this series of tests is shown starting at ≈170-250°C.

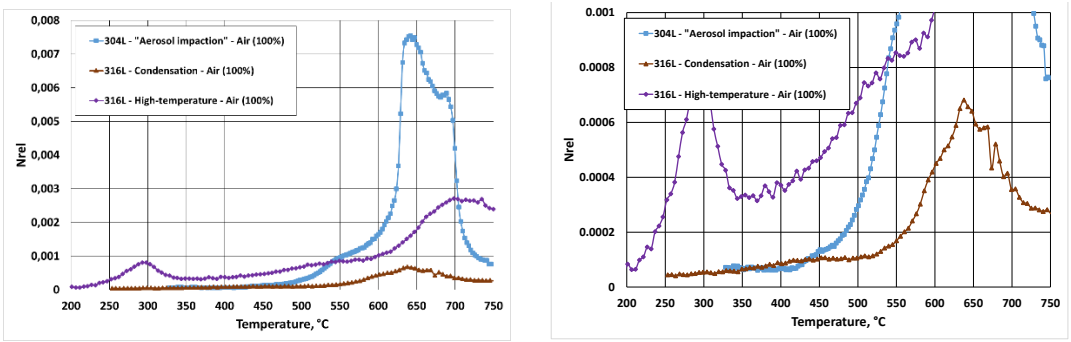

Figure 6. Release and transport kinetics of I_2 during re-vaporization of CsI deposits in pure air with a heating rate of 5°C/min up to 750°C; blue curve : CsI RT aerosol impaction" (condition 1, air flow rate 53 mL_n/min), brown curve: CsI vapour condensation (condition 9, air flow rate 200 mL_n/min); purple curve : CsI high-temperature vapour deposition (condition 6, air flow 200 mL_n/min)

4.2.3. Influence of substrate nature: stainless steel vs. gold inert surface (condition 14)

A previous study [49] has linked the formation of gaseous molecular iodine to the interaction between CsI and Cr_2O_3 in presence of dioxygen. This assumption is supported by the fact that the reaction cited by Sasaki *et al.* [49] is thermodynamically favoured in the temperature range of our conditions. In air conditions, our observations (release of I_2 and formation of caesium chromate species) allowed us to propose a similar reactivity with the surface [31]. For the further understanding of the phenomenon, it was decided to perform additional tests whose goals were to determine whether there are other mechanisms involved in the formation of I_2, besides CsI-substrate interaction.

Consequently, CsI aerosol deposits (aerosol impaction at room temperature) have been generated on a chemically inert surface – gold coupons, and a series of re-vaporization tests in pure air have been performed afterwards (condition n°14). Integral tests in the RIGolo device have led to the total release of caesium (0.4% detected on the coupon after re-vaporization by ICP-MS) and iodine from the surface of the gold coupon. The Cs/I ≈ 1.6 in the alumina tube, suggesting again the re-vaporization of Cs under other species besides CsI compounds. Up to 28% of iodine has been released as I_2 (relative to the total measured amount of iodine at the end of test), which is lower compared to the re-vaporization from the pre-oxidized 304L coupons and 316L foils in the same conditions (conditions 1 and 12 respectively). Nevertheless, this lower release may be owed to deposit inhomogeneities. These results suggest that the formation of I_2 is not due only to the interaction of CsI with the oxide substrate, but that the oxidation of iodide by the gas phase plays an important role in iodine vaporization.

From a kinetic point of view, TGA analysis has shown that the process is initiated at a higher temperature (526°C) compared to CsI re-vaporization onset on 304L coupons (see section 4.2.1). Figure 7 shows the gaseous molecular iodine release kinetics and the pattern clearly resembles that of CsI re-vaporization from pre-oxidized stainless steel surface (condition n°1):

1) A low release between ≈450-560°C;
2) A more important release (up to the depletion of the iodine source) above 560°C. It is worth noting that this release is slower compared to the release in condition n°1.

This suggests that the mechanisms governing the formation of I_2 are very close, regardless of the substrate. As a consequence, the role of pre-oxidized stainless steel in the production of gaseous iodine species is less important than initially expected.

Nevertheless, the differences observed between kinetic of I_2 productions when considering an inert surface and pre-oxidized stainless steel, indicates that some substrate effect cannot be excluded at high temperature.

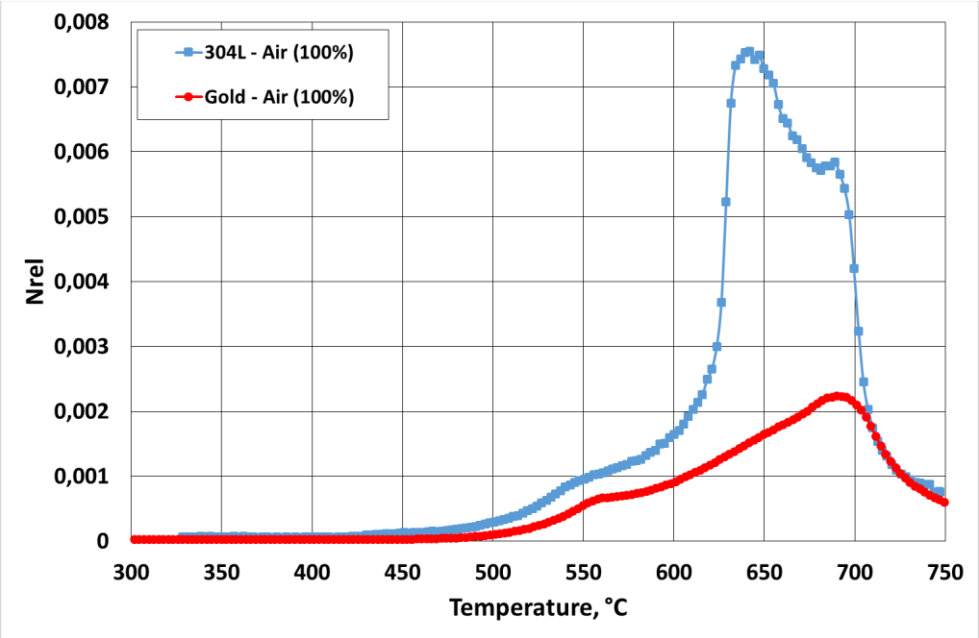

Figure 7. Release and transport kinetics of I_2 during re-vaporization of CsI aerosols (RT aerosol impaction) in pure air (53 53 mLn/min) and with a heating rate of 5°C/min up to 750°C; blue curve: pre-oxidized 304L surface ; red curve : gold surface.

4.2.4. Thermal cycle boundaries : kinetic of I_2 release up to 550°C

Based on the results of previous online measurement tests, it was decided to conduct another one with a limited maximum temperature of ≈550°C, which is the upper limit for the first step of I_2 release. The goal was to study the release phenomenon in the 450-550°C range. In order to reduce the carrier gas interference at low temperature, the sample was heated under argon up to ≈420°C, and then the carrier gas was switched to a mixture of air/steam (% vol. 50/50). Figure 7 shows the I_2 release and transport kinetics and it can be noticed that the release starts at ≈440°C and ends just after the final temperature of ≈550°C is reached, with a subsequent decrease in signal, which is probably due to the depletion of the source involved in this first mechanism. The fine peak at 420°C is an artifact in the IBBCEAS response due to a transient overpressure in the IBB CEAS cell when switching the carrier gas composition from argon to the air/steam mix. This transient induced a shit in the baseline which could not be corrected during the test. The I_2 spectral fingerprint is indeed clearly observed from 450°C on.

No integral test in the RIGolo device has been performed in these conditions, but surface characterization by ToF-SIMS of the sample has been done. The depth profile analysis in positive polarity revealed an intense Cs^+ signal (Figure 8a), while the analysis in negative polarity has revealed the presence of relatively intense I^- secondary ions (Figure 8b). Also, the secondary ion clusters

601 $Cs_2CrO_3^+$ and $Cs_2Cr_2O_9H^+$ have been detected, which indicates the formation of Cs-Cr-O compounds.
602 All these results suggest that a part of iodine has been released from the surface as I_2 and that
603 caesium mainly remained on the surface, both as CsI and mixed Cs-Cr oxides. Furthermore, it would
604 seem that up to 550°C the formation of I_2 is based on the reaction between the CsI deposit and
605 carrier gas components in a heterogeneous phase. The most intense release observed above 550°C
606 (Figure 3, blue curve) could then be explained by the vaporization of CsI deposits (which starts
607 between 550 and 600°C) followed by a reaction in gaseous (homogeneous) phase, which would
608 favour the contact between CsI and carrier gas molecules. In this latter case, the residual quantity of
609 Cs on the surface would be low as observed in condition 1 (see table 3).

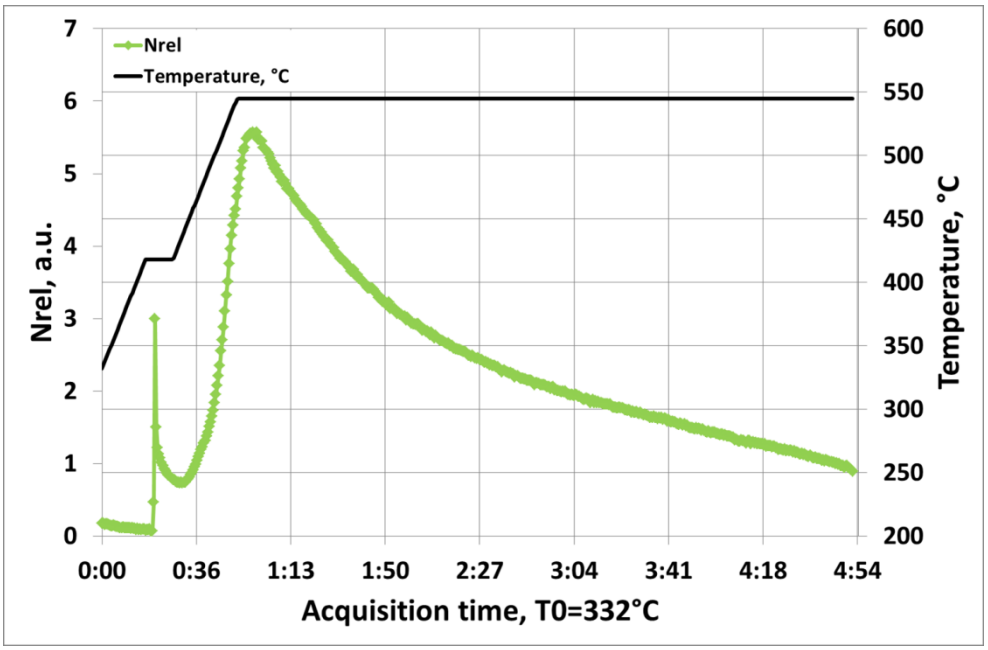

610

611 **Figure 8. Release and transport kinetics of I_2 during re-vaporization of CsI aerosols (RT aerosol impaction) from pre-**
612 **oxidized 304L coupon. Thermal cycle and carrier gas composition: 1) heating up to 420°C in argon; 2) maintain for 10 min**
613 **at 420°C, switching to air/steam (% vol. 50/50); 3) heating up to 550°C and 4) maintain at 550°C for 6h. Gas flow**
614 **200mL$_n$/min. Heating up at 5°C/min.**

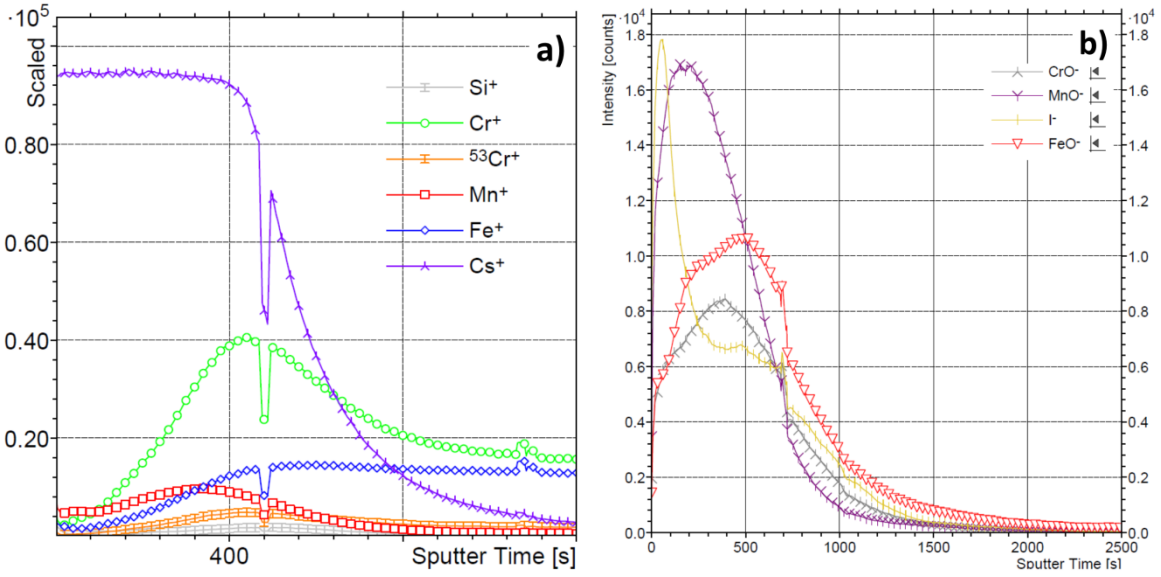

Figure 9. ToF-SIMS depth profile of a CsI aerosol deposit re-vaporized from pre-oxidized 304L coupon: a) secondary ions in positive polarity and b) secondary ions in negative polarity.

5. Theoretical modelling

In order to get insight in the molecular mechanism of the CsI revaporisation for small aerosols, we performed DFT modelling of the possible oxygen interaction and reaction on the surface of the CsI Aerosol. The size of the particle deposited in the experiment is large (larger than 1 µm). The larger part of the CsI particles will not be directly in interaction with the support. Furthermore, the evolution at relatively low temperatures (500 – 650 °C) is mostly independent of the nature of the support. A theoretical model that does not include explicitly the support will be valid to investigate the CsI surface oxidation mechanism. Furthermore, the reactivity of the deposited CsI depends on the preparation conditions which will modify both the size of the particles and the nature of the exposed surfaces and sites. By defining various models of the CsI surfaces, it will be possible to explain the differences observed experimentally as well as the effect of O_2 and water on the surfaces.

5.1. Model

CsI crystal has a simple cubic structure which belongs to the Pm3m group, with two atoms in the unit cell, caesium at (0, 0, 0) and iodine at (a/2) (1, 1, 1) while 'a' being the lattice constant (456.67 pm)[50] kept fixed in the calculation at the experimental. The nature of the exposed surface is defined by the surface energy of low index surfaces. In order to compute them, we define super-cell composed of at least 8 layer of CsI and added 15 Å of vacuum to avoid any interaction between the slab. The four outermost layers have been relaxed. The surface energies of low index surfaces are summarized in table 4.

Table 4 : Surface energy ($mJ.m^{-2}$) after relaxation of low index surfaces.

Surface index	(011)	(111)	(210)	(211)	(001)
Surface energy ($mJ.m^{-2}$)	193	520	365	417	615

The (011) surface is the most stable one and considering the large surface energy difference, it will be the only surface exposed by dehydrated CsI particles. The (011) surface is composed of alternating rows of Cs and I anions.

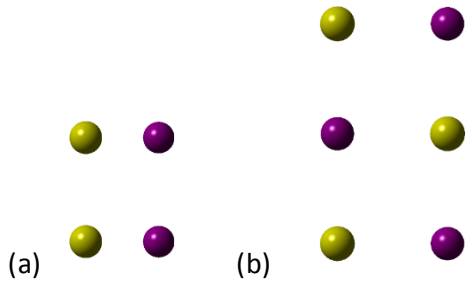

Figure 10. Top (a) and side (b) view of the (011) surface (most stable surface)(Cs in yellow, I in purple).

5.2. H_2O and O_2 Interaction with perfect (011) surfaces.

The reactive molecules in the gas phase during the experiments are water and dioxygen. We studied theoretically the interaction of these two molecules with the CsI surfaces to determine the reaction that may occur on the surface and may explain the iodine revaporisation.

The water absorption on the surface is molecular. One hydrogen atom of the water molecule forms a hydrogen bond with the surface iodine while the negatively charged oxygen atom interacts with the Cs cation. The Cs-O and H-I distances are 3.16 and 2.45 Å respectively. The adsorption energy is 0.52 eV. The adsorption is exothermic but as the main interaction is a weak hydrogen bond, the water molecule adsorption will not be favoured at high temperature. We tested the dissociative adsorption of the water molecule on the surface to form both Cs-OH and HI groups. This adsorption is very endothermic (-3,54 eV). The formation of IH groups on the perfect surface is not possible and such we can exclude the departure of HI(g) molecule from the surface.

Figure 11. Water adsorption on the perfect (011) surface (a) molecular adsorption (b) dissociative adsorption (Cs in yellow, I in purple, O in red, H in white).

The oxygen molecule adsorption on the surface is also a molecular one. The O_2 molecule is located in a $\eta 2$ geometry, on top of one Cs cation. The O-Cs distances are 3.04 A and the O-O one is 1.24 very close to the O-O distance in the gas phase (. The adsorption is endothermic (Eads = -0.18 eV). We study the dissociative adsorption. The oxygen atoms are located in the first surface plane, between Cs and I ion. This adsorption mode is even more endothermic (Eads= -0.88 eV) than the molecular one. The oxygen adsorption and reaction with a perfect surface is not probable at high temperature.

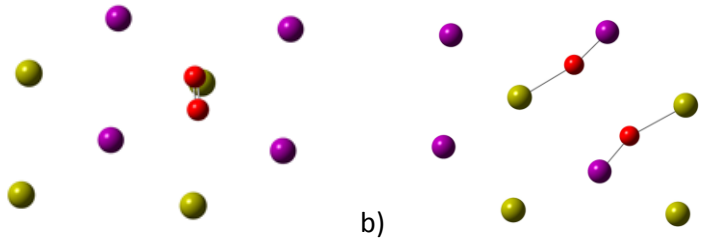

(a) b)

Figure 12. O_2 adsorption on the perfect (011) surface (a) molecular adsorption (b) dissociative adsorption (Cs in yellow, I in purple, O in red).

5.3. O_2 interaction with defective surfaces.

The presence of defects on the surface increases their reactivity. To model these defects, we study the O_2 interaction with a step (011) surface: i.e. the (014) surface, composed a step and a (011) terrace (figure 13). The iodine ions located on the step are under-coordinated which would increase their reactivity.

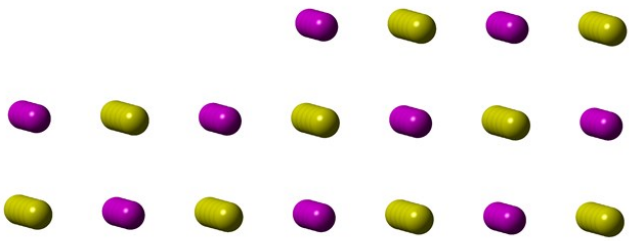

Figure 13. Side view of the stepped (014) surface (Cs in yellow, I in purple).

On the opposite to the perfect surface, the oxygen molecular adsorption on the iodine ion located on the step is an exothermic process (ΔE= -0,57 eV/Eads = 0.57eV) (b step, figure 14) . The oxygen molecule is located between two iodine anions of the edge. The I-O distance is 2.86 Å and the O-O one is 1.27 Å, 0.04 Å larger than the distance for the gas phase molecule. The oxygen molecule is activated when adsorbed on a defect. The dissociative adsorption is favoured on the edge. The adsorption energy is then 1,07 eV (c step , figure 14) . One the oxygen molecule is dissociated on the surface, the desorption of $IO^{\bullet}$ radical is possible. This final step is endothermic (d step , figure 14) but will be favoured by a very concentration of iodine in the gas and by the continuous gas flow above the surface. $IO^{\bullet}$ being a strong oxidant it will react with the iodide to produce $I_{2(g)}$ as demonstrated in liquid [51] and in the gas phase[52].

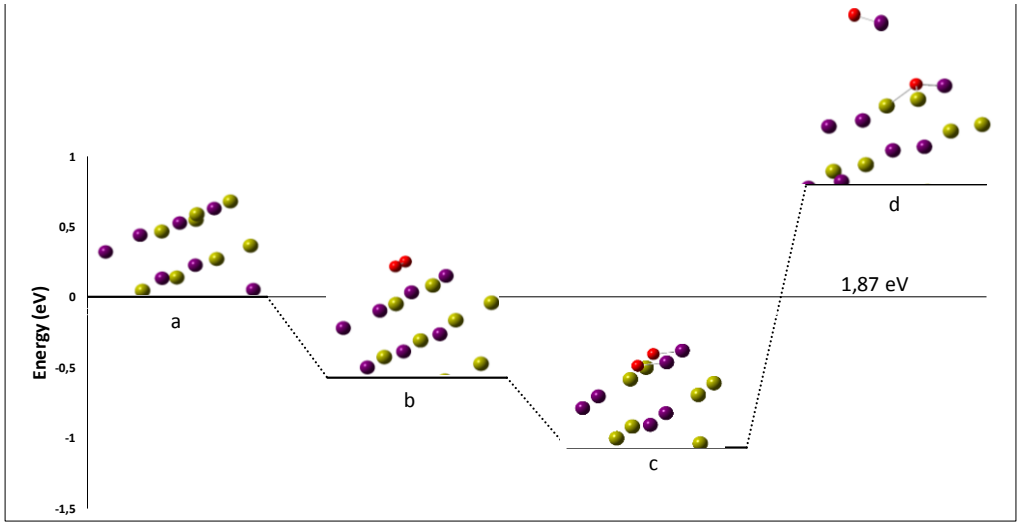

Figure 14. Adsorption and dissociation of O2 on stepped surface (Cs in yellow, I in purple, O in red).

In order to get insight in the kinetic of the oxygen molecule dissociation on the surface, we computed the activation energy of the reaction (figure 15). The activation energy is small (E_{act}= 0,64 eV), which indicate that the surface oxidation will be fast on defects. The O-O distance on the transition state is 1.77 Å.

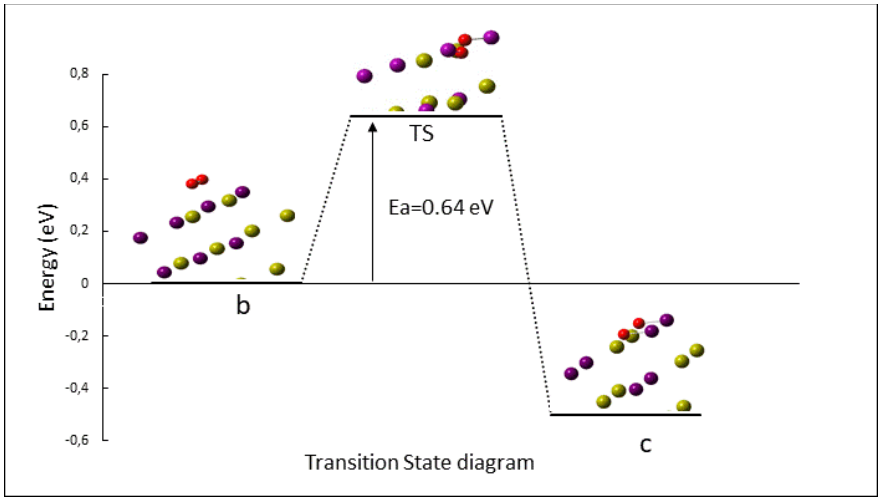

Figure 15. O_2 activation mechanism on the step surface ((Cs in yellow, I in purple, O in red).

From the DFT calculation, we can conclude that the water molecule will not be involved directly in the CsI oxidation reactions and in the I_2 formation. However, when the quantity of water in the feed is much larger than the oxygen one, the water will have a competitive adsorption on the surface.

On the opposite to water, the O2 molecules can react on the CsI particles to form in the first step the radical species $IO^{\bullet}$, but this process will mainly occur on the surface defects. The oxygen reactivity depends then of the nature of the surface and on the numbers of defects. However, once the $IO^{\bullet}$ radical have been formed, this reactive species may react with the surface and such create defects on the particle surface. This mechanism may be responsible for the very fast increase of the reaction rate with temperature that is observed experimentally. It may be mentioned that the CsI reactivity at low temperature (around 400° C according to the experiments) will depend on the exact nature of the surface and on the

deposition method. A fast cooling of hot particles on the surface will favour the formation of defects and increased its reactivity.

6. Conclusion

From the experimental study, the following trends can be summarized as follows:

- In presence of air, the re-vaporization of CsI deposits from pre-oxidized stainless steel surfaces leads to the release of 45-75% of I_2 from initial iodine inventory – except for CsI deposit by vapour condensation. A part of Cs is retained on the surface (2.5-10% of initial amount) and forms mixed Cs-Cr-O compounds;
- In a mixed air/steam atmosphere, between 12-33% of iodine is released as I_2, regardless of the air content in the carrier gas, the molecular iodine fraction probably depends ~~on air content and~~ temperature deposits ;
- The deposit nature (aerosol, high temperature vapour deposition and vapour condensation) does not seem to influence the amount of released molecular iodine strongly or retained caesium. An exception is the CsI deposit by vapour condensation (620-440°C) which is crystalline and thus has an organized structure;
- The re-vaporization of CsI aerosols from an inert surface (gold) in air leads to the formation of 28% of molecular iodine (relative to I initial amount), which is lower compared to the re-vaporization from a stainless steel surface;
- The gaseous molecular iodine release kinetic pattern is generally the same, regardless of carrier gas composition, deposit or substrate nature and consists of two steps: an initial reduced release between ≈440-550°C and a second rapid release above 550°C. In the case of CsI high-temperature deposits (720-620°C) there is an additional I_2 release peak between 200-350°C.

The analysis of these results allows us to make the following conclusions and hypotheses:

- There seem to be several mechanisms responsible for I_2 formation, depending on the temperature. Below 550°C the results suggest a solid-gas (heterogeneous) phase interaction between the deposit and the carrier gas. Above 550°C, the CsI starts to vaporize and the interaction is in gas (homogeneous) phase, which would explain the increased rate of I_2 release;
- The iodine formation is favoured on the CsI surface defects, and such is influenced by the CsI deposition process. The I_2 formation start at higher temperature on well crystallized particles. However, the formation of the first I_2 molecules will induce the formation of defects on the surface which will increase the surface oxidation rate.

To develop some models and cover severe accident boundary conditions, additional experimental investigations are needed to explore other fission products and other gas composition.

Acknowledgements

This work was performed in the frame of the French research program ANR-11-RSNR-0013-01 called MiRE (Mitigation of outside releases in case of nuclear accident), with the financial support of EDF and Framatome. The authors thank the HPC centre of the Lille University for providing CPU resources. Surface analysis have been performed at the 'plateforme d'analyses de surfaces' of the Lille University.

768

769 References

770 1. Cantrel L, Cousin F, Bosland L, et al (2014) ASTEC V2 severe accident integral code: Fission
771 product modelling and validation. Nuclear Engineering and Design 272:195–206.
772 https://doi.org/10.1016/j.nucengdes.2014.01.011

773 2. Haste T, Payot F, Bottomley PDW (2013) Transport and deposition in the Phébus FP circuit.
774 Annals of Nuclear Energy 61:102–121. https://doi.org/10.1016/j.anucene.2012.10.032

775 3. Cantrel L, Albiol T, Bosland L, et al (2018) Research Works on Iodine and Ruthenium Behavior in
776 Severe Accident Conditions. Journal of Nuclear Engineering and Radiation Science 4:020903.
777 https://doi.org/10.1115/1.4038223

778 4. Hidaka A, Igarashi M, Hashimoto K, et al (1995) Experimental and Analytical Study on the
779 Behavior of Cesium Iodide Aerosol/Vapor Deposition onto Inner Surface of Pipe Wall under
780 Severe Accident Conditions. Journal of Nuclear Science and Technology 32:1047–1053.
781 https://doi.org/10.1080/18811248.1995.9731813

782 5. Maruyama Y, Shibazaki H, Igarashi M, et al (1999) Vapor Condensation and Thermophoretic
783 Aerosol Deposition of Cesium Iodide in Horizontal Thermal Gradient Pipes. Journal of Nuclear
784 Science and Technology 36:433–442. https://doi.org/10.1080/18811248.1999.9726226

785 6. Girault N, Payot F (2013) Insights into iodine behaviour and speciation in the Phébus primary
786 circuit. Annals of Nuclear Energy 61:143–156. https://doi.org/10.1016/j.anucene.2013.03.038

787 7. Katata G, Chino M, Kobayashi T, et al (2015) Detailed source term estimation of the
788 atmospheric release for the Fukushima Daiichi Nuclear Power Station accident by coupling
789 simulations of an atmospheric dispersion model with an improved deposition scheme and
790 oceanic dispersion model. Atmospheric Chemistry and Physics 15:1029–1070.
791 https://doi.org/10.5194/acp-15-1029-2015

792 8. Terada H, Katata G, Chino M, Nagai H (2012) Atmospheric discharge and dispersion of
793 radionuclides during the Fukushima Dai-ichi Nuclear Power Plant accident. Part II: verification
794 of the source term and analysis of regional-scale atmospheric dispersion. Journal of
795 Environmental Radioactivity 112:141–154. https://doi.org/10.1016/j.jenvrad.2012.05.023

796 9. Anderson, A., Auvinen, A., Bottomley, P., Bryan, C., Freemantle, N., Hieraut, J., Jokiniemi, J.,
797 Kingsbury, A., & Tuson, A. (2000). Revaporisation tests on samples from Phebus fission
798 products: Final report. (Issue 2 ed.) AEA Technology Report, No. AEAT/R/NS/0124

799 10. Auvinen A, Lehtinen KEJ, Enriquez J, et al (2000) VAPORISATION RATES OF CsOH AND CsI IN
800 CONDITIONS SIMULATING A SEVERE NUCLEAR ACCIDENT. Journal of Aerosol Science 31:1029–
801 1043. https://doi.org/10.1016/S0021-8502(00)00027-6

802 11. Bottomley PDW, Knebel K, Van Winckel S, et al (2014) Revaporisation of fission product
803 deposits in the primary circuit and its impact on accident source term. Annals of Nuclear Energy
804 74:208–223. https://doi.org/10.1016/j.anucene.2014.05.011

805 12. Knebel K, Bottomley PDW, Rondinella VV, et al (2014) An experimental device to study the
806 revaporisation behaviour of fission product deposits under severe accident conditions. Progress
807 in Nuclear Energy 72:77–82. https://doi.org/10.1016/j.pnucene.2013.07.022

13. Kalilainen J, Kärkelä T, Zilliacus R, et al (2014) Chemical reactions of fission product deposits and iodine transport in primary circuit conditions. Nuclear Engineering and Design 267:140–147. https://doi.org/10.1016/j.nucengdes.2013.11.078

14. Shibazaki H, Maruyama Y, Kudo T, et al (2001) Revaporization of a CsI Aerosol in a Horizontal Straight Pipe in a Severe Accident Condition. Nuclear Technology 134:62–70. https://doi.org/10.13182/NT01-A3186

15. Berdonosov s. s., Sitova m. a. (1997) Chemical Forms of Iodine Occurring at Evaporation and Condensation of Cesium Iodide in Air. Radiochemistry 39:341–342

16. Berdonosov s. s., Baronov s. b. (1999) Interaction of caesium Iodide with an Air Flow at High Temperatures. Radiochemistry 41:63–66

17. Kulyukhin SA, Mikheev NB, Kamenskaya AN, et al (2004) Oxidative Hydrolysis in Water Vapor-Air Phase of CsI Radioaerosols Produced by CsI Sublimation from Metallic Surface. Radiochemistry 46:63–66. https://doi.org/10.1023/B:RACH.0000024639.33411.68

18. Hijazi H (2017) RÉACTIVITÉ CHIMIQUE DES AÉROSOLS D'IODE EN CONDITIONS ACCIDENTELLES DANS UN RÉACTEUR NUCLÉAIRE. Université de Lille

19. Khanniche S, Louis F, Cantrel L, Černušák I (2017) Investigation of the Reaction Mechanism and Kinetics of Iodic Acid with OH Radical Using Quantum Chemistry. ACS Earth and Space Chemistry 1:227–235. https://doi.org/10.1021/acsearthspacechem.7b00038

20. Khanniche S, Louis F, Cantrel L, Černušák I (2017) Thermochemistry of HIO_2 Species and Reactivity of Iodous Acid with OH Radical: A Computational Study. ACS Earth and Space Chemistry 1:39–49. https://doi.org/10.1021/acsearthspacechem.6b00010

21. Villard A, Khanniche S, Fortin C, et al (2019) A theoretical study of the microhydration processes of iodine nitrogen oxides. International Journal of Quantum Chemistry 119:e25792. https://doi.org/10.1002/qua.25792

22. Khiri D, Vandeputte R, Taamalli S, et al (2019) Microhydration of caesium metaborate: structural and thermochemical properties of CsBO2 + n H2O (n = 1–4) aggregates. Journal of Molecular Modeling 25:. https://doi.org/10.1007/s00894-019-4094-4

23. Khanniche S, Louis F, Cantrel L, Černušák I (2016) Computational study of the I2O5+ H2O = 2 HOIO2 gas-phase reaction. Chemical Physics Letters 662:114–119. https://doi.org/10.1016/j.cplett.2016.09.023

24. Khanniche S, Louis F, Cantrel L, Černušák I (2016) A theoretical study of the microhydration of iodic acid (HOIO2). Computational and Theoretical Chemistry 1094:98–107. https://doi.org/10.1016/j.comptc.2016.09.010

25. Khanniche S, Louis F, Cantrel L, Černušák I (2016) A Density Functional Theory and *ab Initio* Investigation of the Oxidation Reaction of CO by IO Radicals. The Journal of Physical Chemistry A 120:1737–1749. https://doi.org/10.1021/acs.jpca.6b00047

26. Sudolská M, Cantrel L, Budzák Š, Černušák I (2014) Molecular structures and thermodynamic properties of monohydrated gaseous iodine compounds: Modelling for severe accident simulation. Journal of Nuclear Materials 446:73–80. https://doi.org/10.1016/j.jnucmat.2013.11.029

27. Sudolská M, Cantrel L, Černušák I (2014) Microhydration of caesium compounds: Cs, CsOH, CsI and Cs2I2 complexes with one to three H2O molecules of nuclear safety interest. Journal of Molecular Modeling 20:. https://doi.org/10.1007/s00894-014-2218-4

28. Šulková K, Cantrel L, Louis F (2015) Gas-Phase Reactivity of Cesium-Containing Species by Quantum Chemistry. The Journal of Physical Chemistry A 119:9373–9384. https://doi.org/10.1021/acs.jpca.5b05548

29. Taamalli S, Khiri D, Suliman S, et al (2020) Unraveling the Tropospheric Microhydration Processes of Iodous Acid HOIO. ACS Earth and Space Chemistry 4:92–100. https://doi.org/10.1021/acsearthspacechem.9b00257

30. Giordano P, Auvinen A, Brillant G, et al (2010) Recent advances in understanding ruthenium behaviour under air-ingress conditions during a PWR severe accident. Progress in Nuclear Energy 52:109–119. https://doi.org/10.1016/j.pnucene.2009.09.011

31. Obada D., Gasnot L, Mamede A-S, Grégoire A-C (2017) Assessment of medium-term radioactive releases in case of a severe nuclear accident on a Pressurized Water Reactor: experimental study of fission products re-vaporization from deposits (Cs,I). In: Proceedings of ICAPP 2017. Atomic Energy Society of Japan, Fukui and Kyoto (Japan), p 17328

32. Mamede A-S, Nuns N, Cristol A-L, et al (2016) Multitechnique characterisation of 304L surface states oxidized at high temperature in steam and air atmospheres. Applied Surface Science 369:510–519. https://doi.org/10.1016/j.apsusc.2016.01.185

33. Obada D, Mamede A-S, Nuns N, et al (2018) Combined ToF-SIMS and XPS characterization of 304L surface after interaction with caesium iodide under PWR severe accident conditions. Applied Surface Science 459:23–31. https://doi.org/10.1016/j.apsusc.2018.07.212

34. Johansson O, Mutelle H, Parker AE, et al (2014) Quantitative IBBCEAS measurements of I2 in the presence of aerosols. Applied Physics B 114:421–432. https://doi.org/10.1007/s00340-013-5536-9

35. Obada D (2017) Evaluation de rejets moyen-terme en situation accidentelle grave d'un Réacteur à Eau Pressurisée : étude expérimentale de la re-vaporisation de dépôts de produits de fission (Cs, I). Université de Lille

36. Gouello M, Mutelle H, Cousin F, et al (2013) Analysis of the iodine gas phase produced by interaction of CsI and MoO3 vapours in flowing steam. Nuclear Engineering and Design 263:462–472. https://doi.org/10.1016/j.nucengdes.2013.06.016

37. Grégoire A-C, Kalilainen J, Cousin F, et al (2015) Studies on the role of molybdenum on iodine transport in the RCS in nuclear severe accident conditions. Annals of Nuclear Energy 78:117–129. https://doi.org/10.1016/j.anucene.2014.11.026

38. Bahrini C, Grégoire A-C, Obada D, et al (2018) Incoherent broad-band cavity enhanced absorption spectroscopy for sensitive and rapid molecular iodine detection in the presence of aerosols and water vapour. Optics & Laser Technology 108:466–479. https://doi.org/10.1016/j.optlastec.2018.06.050

39. vasp.5.4.1

40. Hafner J (2008) *Ab-initio* simulations of materials using VASP: Density-functional theory and beyond. Journal of Computational Chemistry 29:2044–2078. https://doi.org/10.1002/jcc.21057

41. Kresse G, Furthmüller J (1996) Efficiency of ab-initio total energy calculations for metals and semiconductors using a plane-wave basis set. Computational Materials Science 6:15–50. https://doi.org/10.1016/0927-0256(96)00008-0

42. Kresse G, Joubert D (1999) From ultrasoft pseudopotentials to the projector augmented-wave method. Physical Review B 59:1758–1775. https://doi.org/10.1103/PhysRevB.59.1758

43. Perdew JP, Burke K, Ernzerhof M (1996) Generalized Gradient Approximation Made Simple. Physical Review Letters 77:3865–3868. https://doi.org/10.1103/PhysRevLett.77.3865

44. Methfessel M, Paxton AT (1989) High-precision sampling for Brillouin-zone integration in metals. Physical Review B 40:3616–3621. https://doi.org/10.1103/PhysRevB.40.3616

45. Monkhorst HJ, Pack JD (1976) Special points for Brillouin-zone integrations. Physical Review B 13:5188–5192. https://doi.org/10.1103/PhysRevB.13.5188

46. Tkatchenko A, Scheffler M (2009) Accurate Molecular Van Der Waals Interactions from Ground-State Electron Density and Free-Atom Reference Data. Physical Review Letters 102:. https://doi.org/10.1103/PhysRevLett.102.073005

47. Riggs CA, Tompson RV, Ghosh TK, et al (2007) Water Adsorption Isotherms for Charged and Uncharged Cesium Iodide Aerosol Particles. Nuclear Technology 157:74–86. https://doi.org/10.13182/NT07-A3803

48. Souvi SMO, Badawi M, Virot F, et al (2017) Influence of water, dihydrogen and dioxygen on the stability of the Cr2O3 surface: A first-principles investigation. Surface Science 666:44–52. https://doi.org/10.1016/j.susc.2017.08.005

49. Sasaki K, Tanigaki T, Tomohiro Oshima, et al (2013) Microstructure Analysis for Chemical Interaction between Cesium and SUS316 Steel in Fast Breeder Reactor Application. Journal of Energy and Power Engineering 7:716–725. https://doi.org/10.17265/1934-8975/2013.04.014

50. Satpathy S (1986) Electron energy bands and cohesive properties of CsCl, CsBr, and CsI. Physical Review B 33:8706–8715. https://doi.org/10.1103/PhysRevB.33.8706

51. Sakamoto Y, Yabushita A, Kawasaki M, Enami S (2009) Direct Emission of I_2 Molecule and IO Radical from the Heterogeneous Reactions of Gaseous Ozone with Aqueous Potassium Iodide Solution. J Phys Chem A 113:7707–7713. https://doi.org/10.1021/jp903486u

52. Fortin C, Fèvre-Nollet V, Cousin F, et al (2019) Box modelling of gas-phase atmospheric iodine chemical reactivity in case of a nuclear accident. Atmospheric Environment 214:116838. https://doi.org/10.1016/j.atmosenv.2019.116838